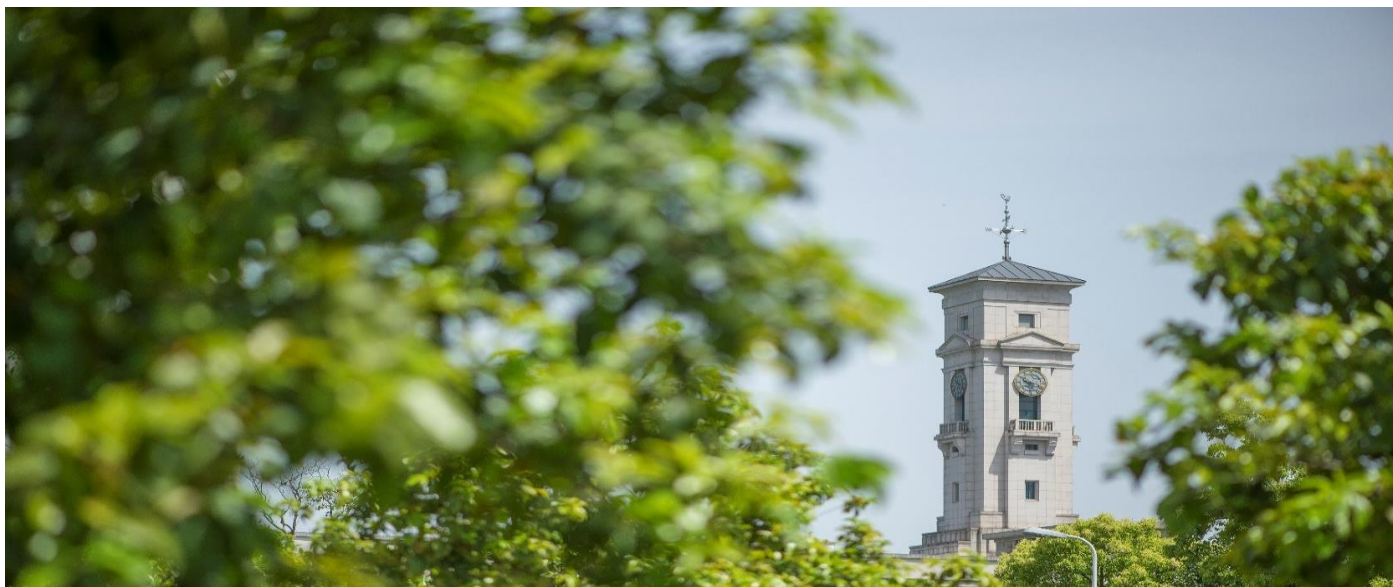


Opposite Effects of Co and Cu Dopants on the Catalytic Activities of Birnessite MnO₂ Catalyst for Low-Temperature Formaldehyde Oxidation

Abubakar Yusuf, Yong Sun, Yong Ren, Colin Snape, Chengjun Wang,
Hongpeng Jia, Jun He



**University of
Nottingham**

UK | CHINA | MALAYSIA

University of Nottingham Ningbo China, 199 Taikang East Road, Ningbo, 315100, Zhejiang, China.

First published 2020

This work is made available under the terms of the Creative Commons Attribution 4.0 International License:

<http://creativecommons.org/licenses/by/4.0>

The work is licenced to the University of Nottingham Ningbo China under the Global University Publication Licence:

<https://www.nottingham.edu.cn/en/library/documents/research/global-university-publications-licence-2.0.pdf>



**University of
Nottingham**

UK | CHINA | MALAYSIA

Opposite Effects of Co and Cu Dopants on the Catalytic Activities of Birnessite MnO₂ Catalyst for Low-Temperature Formaldehyde Oxidation

Abubakar Yusuf^{a,b}, Yong Sun^b, Yong Ren^c, Colin Snape^d, Chengjun Wang^e, Hongpeng Jia^f, Jun He^{a,b,}*

^a International Doctoral Innovation Center, University of Nottingham Ningbo China, Ningbo, China

^b Department of Chemical and Environmental Engineering, University of Nottingham Ningbo China, Ningbo, China

^c Department of Mechanical, Materials and Manufacturing Engineering, University of Nottingham Ningbo China, Ningbo, China

^d Faculty of Engineering, University of Nottingham, University Park, Nottingham, United Kingdom

^e College of Resources and Environmental Science, South-Central University for Nationalities, Wuhan, China

^f Institute of Urban Environment, Chinese Academy of Sciences, Xiamen, China

Keywords: doped birnessite MnO₂; doping; Copper; Cobalt; formaldehyde; catalytic oxidation

ABSTRACT: Defect engineering is an effective strategy to enhance the activity of catalysts for various application. Herein, it was demonstrated that in addition to enhancing surface properties via doping, the influence of dopants on the surface-intermediates interaction is a critical parameter that impact catalytic activity of doped catalysts for low-temperature formaldehyde (HCHO) oxidation. The incorporation of Co into the lattice structure of δ -MnO₂ led to the generation of oxygen vacancies, which promoted the formation of surface active oxygen species, reduced activation energy, and enhanced catalytic activity for low-temperature oxidation of HCHO. On the contrary, Cu doping led to a drastic suppression of the catalytic activity of δ -MnO₂, despite its enhanced redox properties and slight increase in the surface concentration of active oxygen species, compared to the pristine δ -MnO₂. Diffuse reflectance infrared Fourier transform (DRIFTS) analysis revealed that in the presence of Cu, carbonate intermediate species accumulate on the surface of the catalysts leading to partial blockage of active sites and suppression of catalytic activity.

1. INTRODUCTION

Volatile organic compounds (VOCs) constitute one of the main sources of air pollutants that pose grievous challenges to human health.¹⁻² Various removal techniques have been devised to eliminate VOCs from the environment, which include adsorption, photocatalysis and catalytic oxidation.³⁻⁴ Amongst these pollutants, formaldehyde (HCHO) is of great interest, because it is one of the most commonly found pollutants in the indoor environment. Its removal is pertinent to improving human health and indoor air quality, as exposure to HCHO can cause adverse health effects and nasopharyngeal cancer in extreme cases.⁵ Catalytic oxidation is a promising technique

that could effectively mineralize HCHO into harmless products: CO₂ and H₂O, and completely remove it from the indoor environment.⁵⁻⁶

Recent attention has focused on the development of cost-effective transition metal based catalysts for various applications in catalysis. Structured manganese oxide (MnO₂) catalysts have been a subject immense research focus as promising cost-effective, active and environmentally friendly alternatives.^{5, 7} Amongst the structured manganese oxide catalysts, birnessite (δ -MnO₂) has received a special attention due to its unique properties. Important characteristics of δ -MnO₂ include its layered structure, mixed oxidation state and charge-neutralizing cations situated in the interlayer spaces. This allows possibilities for further structural modification to enhance its properties and catalytic activity. Various strategies devised, such as defect engineering, have enhanced the properties and catalytic activity of δ -MnO₂ catalysts for various applications including oxidation reactions. Structural defects could be induced through doping or the incorporation of metal cations into the lattice framework of the host material.⁸⁻⁹ The partial substitution of Mn⁴⁺ by dopants within the [MnO₆] octahedral framework of δ -MnO₂ could lead to the generation of oxygen vacancies and structural lattice distortion.¹⁰ These defective sites serve as centers for the adsorption and activation of molecules, and in particular, the generation of active oxygen species, through the activation of water and/or molecular oxygen, which were shown to actively participate in most oxidation reactions, particularly HCHO oxidation.^{7, 11-12} Additionally, dopants can improve the catalytic activity of δ -MnO₂ by enhancing its redox properties and lattice oxygen mobility and reactivity through the reduction of charge transfer resistance.¹³⁻¹⁴

Due to their similar ionic radii, Cobalt (Co) was shown to effectively incorporate into the octahedra of δ -MnO₂ by substituting Mn⁴⁺ leading to the creation oxygen vacancies.¹⁰ Elmaci et al.¹³ explored various transition metals as dopants for δ -MnO₂ and demonstrated that, compared

to the pristine δ -MnO₂, Co-doped δ -MnO₂ exhibited enhanced catalytic activity and chemical stability for water oxidation reaction. This is due to the substitution of Mn⁴⁺ by Co³⁺ in the octahedral framework of δ -MnO₂ leading to an increase in the ration of Mn³⁺/Mn⁴⁺. Similar observations were reported elsewhere for Co doped δ -MnO₂ for water oxidation catalysis.¹⁵ Yin et al.¹⁶ observed that the substitution of Mn⁴⁺ by Co³⁺ resulted in the negative charge of the δ -MnO₂ layers and an increase in the concentration of hydroxyl groups, which accounted for its improved capacity for the adsorption of lead and arsenite from water. The formation of Co-Mn-O and Cu-Mn-O bridges in the case of Co¹⁷ and Cu¹⁸ doped MnO₂ respectively, was shown to improve the mobility and activity of lattice oxygen, which enhances catalytic activity for the preferential oxidation of CO. In another report, Wang et al.¹⁹ investigated the modification of δ -MnO₂ for CO oxidation with various transition metals. They showed that Copper (Cu) doped δ -MnO₂ exhibited improved low temperature activity compared to the pristine catalyst. The substitution of Mn by the dopants facilitated the generation of oxygen vacancies and the mobility of lattice oxygen leading to the generation of more active surface oxygen species. Similar observations were reported for Cu doped δ -MnO₂ for toluene²⁰ and benzene²¹ oxidation, with significantly lower temperature activities compared to the unmodified δ -MnO₂, owing to the formation of oxygen vacancies and its resultant effect on low-temperature reducibility and lattice oxygen reactivity. Doping Cu into the octahedra framework of δ -MnO₂ was also shown to reduce the electron transfer resistance of δ -MnO₂, thereby enhancing its catalytic activity and stability for oxygen reduction reaction.¹⁴ The above works have demonstrated the prospects of Co and Cu as suitable dopants for enhancing the properties and catalytic activity of δ -MnO₂ for HCHO oxidation, as defective sites were demonstrated to improve the redox properties of Mn, and

facilitate the activation and mobility of oxygen into surface active species, which in turn enhances catalytic activity for HCHO.^{8, 22-23}

Besides the enhancement of catalysts' properties induced by doping, the influence of dopants on the surface reaction of intermediates is another critical parameter that influences catalytic activity. It is well known that the surface accumulation of intermediates species grossly affect catalytic activity for reactions such as CO preferential oxidation, and their decomposition and desorption from the surface becomes critical.²⁴⁻²⁶ The type of dopant employed for CO preferential oxidation, was shown to have a tremendous effect on the decomposition of adsorbed intermediates and catalytic activity. For instance, the presence of La, as a dopant, induced the surface accumulation of carbonate intermediates leading to the blockage of active sites and reduced catalytic activity, while a promotional effect was observed in the presence of Nd, for CO preferential oxidation over ceria.²⁵ Similar intermediates poisoning effect was observed on CO oxidation rate when Zr was used as a dopant in CuO/CeO₂.²⁶

Despite recent research works that demonstrated δ -MnO₂ to be an active and cost-effective transition metal catalyst for low-temperature HCHO oxidation,^{5, 7, 11, 27} only a few works were reported on its enhancement, via doping, which include Ce,²² W⁸, and Nb,²⁸ and the doping technique proved positive for enhancing the catalytic of δ -MnO₂. So far, a study that explored the impact of dopants on surface-intermediate interaction and how it affects catalytic activity for HCHO oxidation is rarely reported. Such an understanding is vital in the rational design of active catalysts for practical application in HCHO oxidation, particularly for low to room temperature reactions, in which case, not enough energy is provided to facilitate the desorption of intermediates from the catalyst surface. In this study, Co and Cu were explored as individual dopants for the modification of δ -MnO₂ for low-temperature HCHO oxidation. Co and Cu were selected as model

dopants because: cations with coordination radius similar to that Mn can easily substitute Mn and incorporate into the octahedral framework of δ -MnO₂ leading to the creation of defects,^{8,10} and no previous study, to the best of the authors' knowledge, explored Co and Cu as individual δ -MnO₂ dopants for HCHO oxidation.

Herein, we demonstrated that besides the structure-activity effects of dopants, their influence on surface interaction with intermediates is another critical parameter that determines the catalytic activity of the modified catalysts for HCHO oxidation. Characterization and catalytic activity results revealed that while Co doping exhibited a promotional effect on the catalytic activity of δ -MnO₂, an inhibitory effect was observed in the presence of Cu, leading to the suppression of the catalytic activity of δ -MnO₂ for HCHO oxidation. The structural and the surface properties of the pristine δ -MnO₂ and doped catalysts were investigated by various characterization techniques. In situ Diffuse Reflectance Infrared Fourier Transform (DRIFTS) was used to study the surface reaction and the dopant-intermediates interaction on the surface of the catalyst.

2. EXPERIMENTAL

2.1 Catalysts Synthesis. Microwave-assisted hydrothermal synthesis of δ -MnO₂ was accomplished using MARS 5 Microwave oven (CEM Corporation, USA). A typical synthesis⁷ used 1g of KMnO₄ (Sinopharm) and 0.4g ammonium oxalate (Aladdin) dissolved in 50 ml deionized water and stirred for 30 minutes at room temperature. The resultant solution was transferred into a 100 ml Teflon vessel secured by an explosion-proof Kevlar sleeve assembled into a support module. The synthesis temperature was controlled at 140°C for 30 minutes. After cooling down to room temperature, the formed brown precipitates were filtered under vacuum and washed with deionized water. The precipitates were dried in an oven at 105°C for 12 hrs. The

recovered catalyst was labelled δ -MnO₂. Co and Cu doping into δ -MnO₂ was achieved by separately introducing appropriate amounts of cobalt nitrate and copper nitrate (equivalent to 0.05 mole ratio: x/Mn, x = Co, Cu) into the precursor solutions prior to the microwave treatment. The obtained catalysts were respectively named 0.05Co- δ -MnO₂ and 0.05Cu- δ -MnO₂.

2.2 Characterization. The crystal phases of the synthesized catalysts were identified using X-ray powder diffraction technique (XRD) collected on a D8 Advanced (Bruker, Germany) instrument. Raman spectra were obtained using Renishaw inVia Raman Microscope with an excitation source at 532 nm from 60-1800 cm⁻¹. The morphological structure of the catalysts were observed on Hitachi S-4800 Field Emission Scanning Electron Microscope (FESEM) equipped with EDS for elemental analysis, prior to which samples were sputtered with Pt. TEM and HRTEM images were obtained using a JEM-2100 (JOEL, Japan) instrument. The textural properties of the catalysts were analyzed using a Micrometric 2020 analyzer. Preceding the analysis, samples were degassed at 200°C for 3 hrs, to removed surface adsorbed moisture and gases. Using Kratos Axis Ultra DLS instrument, XPS analysis was conducted to obtain the surface oxidation states and chemical environment of the constituent elements of the catalysts. Elemental compositions were determined using Inductively Coupled Plasma Mass Spectrometry (PerkinElmer). Information on the surface reducibility of the catalysts was obtained on micrometrics Autochem II (chemisorption analyzer) via H₂-TPR. Approximately 50 mg of the catalysts were loaded in a quartz tube, degassed for 1 hr under a flow of 150 ml min⁻¹ Ar. Reduction profile was collected from 30 to 500°C at 5°C min⁻¹ temperature ramp. Information on the surface reaction and intermediates were obtained using in situ diffuse reflectance infrared Fourier transform spectroscopy (DRIFTS) on Thermo fisher, Nicolet 6700 equipped with Praying Mantis reaction cell, at a flow rate of 30 ml min⁻¹ of ~ 75 ppm of HCHO in 21%O₂ balanced in N₂.

2.3 Catalytic Activity Evaluation. The catalytic activity of the catalysts for HCHO oxidation within the temperature range of 30 to 120°C were evaluated. In a typical test, about 50 mg (40 – 60 mesh) of catalyst was weighed and loaded into a fixed bed reactor (6 mm ID). 170 ppm of HCHO was generated by passing air over paraformaldehyde (97% Alfa Aesar) maintained at 30°C in a water bath. The total feed flowrate over the catalyst bed was maintained at 100 ml min⁻¹ (120,000 ml · g⁻¹ · h⁻¹) with a relative humidity (RH) of ~ 50 %. With the aid of an Agilent 7890B GC fitted with an FID and a Polyarc universal carbon detector/reactor (Activated Research Company (ARC), US), the concentration of generated CO₂ and unreacted HCHO in the outlet stream were simultaneously monitored online. CO₂ was the only detected reaction product. The effect of space velocity on catalytic activity was investigated in the GHSV range of 120,000 to 400,000 ml · g⁻¹ · h⁻¹. The stability and room-temperature oxidation of HCHO were investigated at 25°C in a dynamic mode at 60,000 ml g⁻¹ · h⁻¹ in the presence of ~ 10 ppm HCHO concentration (21%O/79%N₂) for 72 hrs. Since CO₂ was the reaction product, the conversion of HCHO (%) was calculated using the equation below:

$$\text{Conversion}(\%) = \frac{\text{CO}_{2\text{out}}}{\text{HCHO}_{\text{in}}} * 100 \dots\dots\dots \text{Eq. (1)}$$

where CO_{2out} and HCHO_{in} represent the outlet concentrations of CO₂ (ppm) and inlet concentration of HCHO (ppm) respectively. To determine the activation energy, the space velocity was varied from 240,000 to 400,000 ml · g⁻¹ · h⁻¹ to maintain the conversion below 20%.

3. RESULTS AND DISCUSSION

3.1 Structure, morphology, and physicochemical properties. The crystal phase of the synthesized MnO₂ catalysts were investigated using XRD measurements (Figure 1). The

diffraction peaks located at 2θ 12.3°, 24.5°, 36.5° and 65.5° can be assigned to the (001), (002), (100) and (110) planes of layered birnessite MnO₂ (JCPDS No. 80–1098) with poor crystallinity. Birnessite MnO₂ with 2D-layer is mainly composed of edge-sharing MnO₆ octahedra with varying amounts of Mn³⁺/Mn⁴⁺, resulting to electrostatic charge imbalance and octahedra vacancies. Positively charged alkali cations such as K⁺ or Na⁺ and water molecules are situated in the interlayer spaces, to provide charge balance, leading to an interlayer spacing of ~ 0.7 nm.²⁹⁻³⁰ All three catalysts possess similar diffraction patterns, with no visible peaks corresponding to Co and Cu, indicating that both Co and Cu are well dispersed/incorporated in the MnO₂. The weak nature of the peaks indicates the poor crystallinity of all catalysts. However, with the addition of dopants, a slight weakening in peak intensity was observed, which might indicate reduction in the crystallinity and structural disorder of the MnO₂. Furthermore, Raman spectra were collected to further understand the local structures of the catalysts and the effects of dopants.

The Raman spectra of the catalysts are presented in Figure 2. All the as-prepared catalysts exhibit three major absorption peaks at around 500 (v₃), 570 (v₂) and 630 cm⁻¹ (v₁) which are the characteristic bands of layered δ-MnO₂. The Raman band at 630 cm⁻¹ could be assigned to the v₁(Mn-O) symmetric stretching vibration of MnO₆ groups while the band at 570 cm⁻¹ is the fingerprint band usually ascribed to the v₂(Mn-O) stretching vibration in the basal plane of MnO₆ sheets of δ-MnO₂ framework. The peak at around 500 cm⁻¹ arises from the flexural vibration of the Mn-O-Mn of the MnO₆ group.³¹ Even after doping with 0.05 Co and Cu, birnessite structure did not collapse as shown in Figure 2, indicating its stability in the presence of dopants at low doping ratio.^{22, 32}

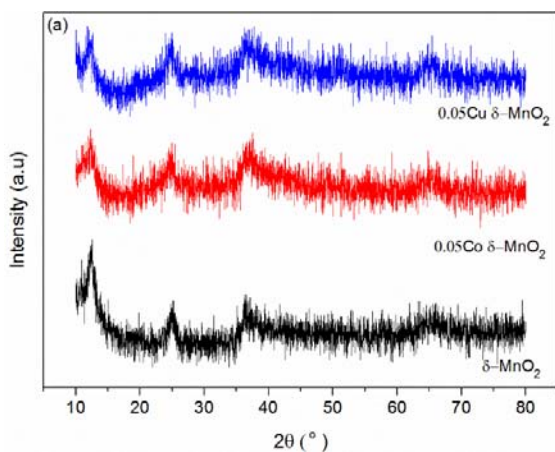


Figure 1. XRD patterns of pristine δ -MnO₂, 0.05Co δ -MnO₂ and 0.05Cu δ -MnO₂.

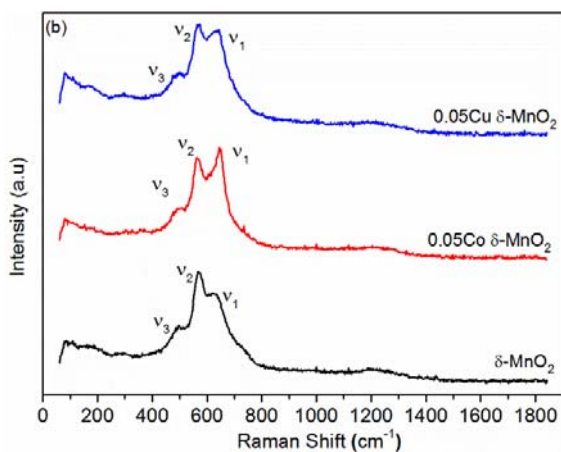


Figure 2. Raman spectra of pristine δ -MnO₂, 0.05Co δ -MnO₂ and 0.05Cu δ -MnO₂

Figure 3 presents the FE-SEM, TEM and HRTEM images of the pristine and doped catalysts. The pristine δ -MnO₂ is composed of entangled nanostrands of an average size of 17.8 nm arranged into nanospheres of about 110 nm. Though the nanospherical morphologies were retained even after doping with Co and Cu, a large degree of particle size reduction into smaller nanospheres of around 37.6 nm were observed in the case of Co, while large, dense and compact aggregated nanospheres with irregular shapes of about 147 nm in size were observed after Cu doping. This could be a result of the incorporation of Co into the lattice structure of birnessite leading to the inhibition of the growth of manganese crystals thereby resulting into smaller particle sizes, which

is accompanied by increase in surface area,²² as shown in Table 1. It was also reported elsewhere that the substitution of Mn ions by V³³⁻³⁴ and Mo³⁵ in the lattice structure of MnO₂ leads to lattice deformation and inhibition of crystal growth, with the formation of smaller particle size. In the case of 0.05Cu- δ -MnO₂, the larger particle sizes and particle agglomerations led to significant reduction in surface area as observed in the FE-SEM (Figure 3g) and BET (Table 1) results, respectively. Similar observations were reported elsewhere for low ratio of Cu doping in MnO₂.³⁶ Additionally, in comparison to the pristine δ -MnO₂, smaller sized nanospheres are evident in the TEM images of 0.05Co- δ -MnO₂ (Figure 3e), while larger nanospheres were observed in 0.05Cu- δ -MnO₂ (Figure 3h), further corroborating the FE-SEM results. The HRTEM images further confirmed the birnessite structure of the catalysts in agreement with the XRD and Raman results. The observed lattice fringes of 0.71 nm corresponds to the (001) plane of birnessite MnO₂. Unlike in the case of the pristine δ -MnO₂, where well resolved lattices fringes were observed along the (001) plane of the nanostrand (Figure 3c), a reduction in lattice periodicity and long-range order was observed in the doped catalysts (Figure 3f and 3i). This could be attributable to structural defects, due to lattice distortions,³⁷⁻³⁸ possibly resulting from incorporation of the dopants into the lattice structure of δ -MnO₂. A higher degree of lattice distortion was observed on 0.05Co- δ -MnO₂ compared to 0.05Cu- δ -MnO₂, likely indicating a higher level of Co incorporation.

Table 1. Surface area and chemical analysis

| Sample Name | BET Surface Area (m ² /g) | EDS (molar) | | | ICP-MS (molar) | |
|------------------------------------|--------------------------------------|-------------|-------|-------------------|----------------|-------|
| | | K/Mn | Mn/O | x/Mn ^a | K/Mn | x/Mn |
| δ -MnO ₂ | 141.3 | 0.17 | 0.472 | - | 0.27 | - |
| 0.05Co- δ -MnO ₂ | 176.3 | 0.18 | 0.396 | 0.043 | 0.29 | 0.047 |
| 0.05Cu- δ -MnO ₂ | 61.8 | 0.17 | 0.434 | 0.042 | 0.25 | 0.045 |

a. x stands for Co and Cu dopants

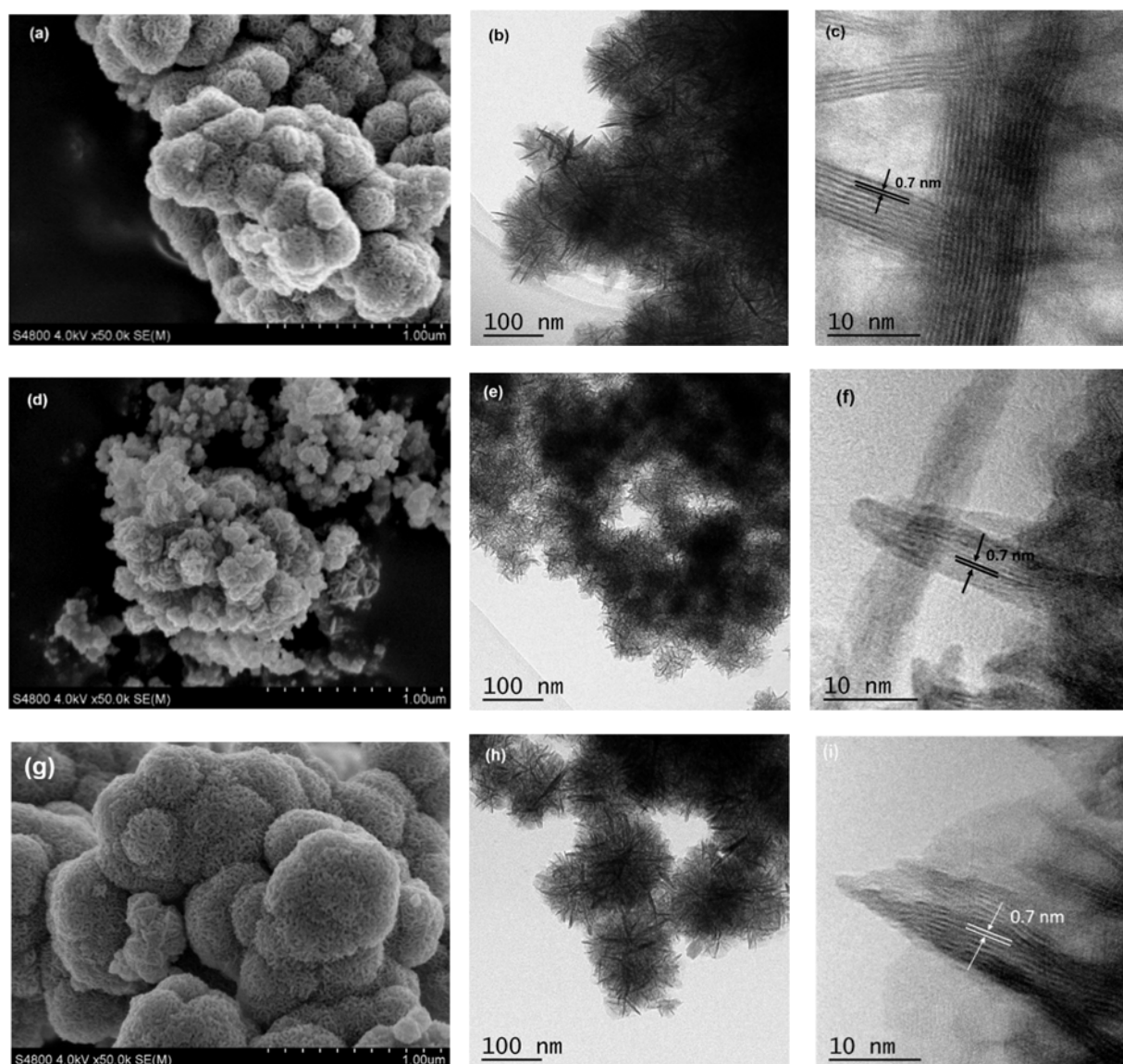


Figure 3. FE-SEM, TEM, HRTEM images of δ -MnO₂ (a-c), 0.05 Co-MnO₂ (d-f), 0.05Cu-MnO₂ (g-i)

The elemental composition of the catalysts are presented in Table 1. Both the EDS and ICP-MS results showed that the experimental amount of dopants present in the catalysts matrix are very close to the theoretical values. The K/Mn ratio of the doped catalysts remain relatively the same as that of the of the pristine catalyst, in both the ICP-MS and EDS results, indicating that the dopants did not replace K⁺ in the interlayer structure of birnessite, but are rather dispersed on or incorporated in the MnO₂ framework. This explains the retained birnessite structure of the doped

catalysts and further supports the sorption of dopants into δ -MnO₂. Similar observation was reported elsewhere for low doping ratio of transition metals in birnessite MnO₂.¹⁹

The XPS results are summarized in Table 2 and depicted in Figure 4. The peaks at around 653.8-653.9 eV and 641.9-643.5 eV are respectively assigned to Mn 2p_{1/2} and Mn 2p_{3/2} splitting. The Mn 2p_{3/2} was further deconvoluted into 2 peaks with centers at 641.9-642.2 eV and 643.3-643.45 eV corresponding to Mn³⁺ and Mn⁴⁺ respectively.^{6, 19, 37} The splitting of Co 2p_{1/2} (795.12 eV) and Co 2p_{3/2} (780.1 eV) (Figure S1) was found to be 15.02 eV, in agreement with the reported values for Co³⁺.¹⁶ The presence of a shakeup peak at around 943 eV and a peak centered at around 933.6 eV (Fig S2) indicates that the doped Cu exists in Cu²⁺ state.³⁹⁻⁴⁰ The observed decrease in the ratio of Mn⁴⁺/Mn³⁺ is due to the substitution of Mn⁴⁺ by the dopants in the lattice of birnessite MnO₂ and indicates the creation of oxygen vacancies. Once Mn⁴⁺ is removed or substituted and Mn³⁺ appears, oxygen vacancies exist to maintain the electrostatic balance in the MnO₂.²² The oxygen vacancies are created by the removal of lattice oxygen to generate anion-vacant sites layers.^{37, 41} Thus, the lower the surface ratio of Mn⁴⁺/Mn³⁺ of the catalysts, the higher the expected oxygen vacancies in the catalyst. Consequently, on the basis of the lowest Mn⁴⁺/Mn³⁺ of 0.05Co δ -MnO₂, it is expected to possess higher density of oxygen vacancies.

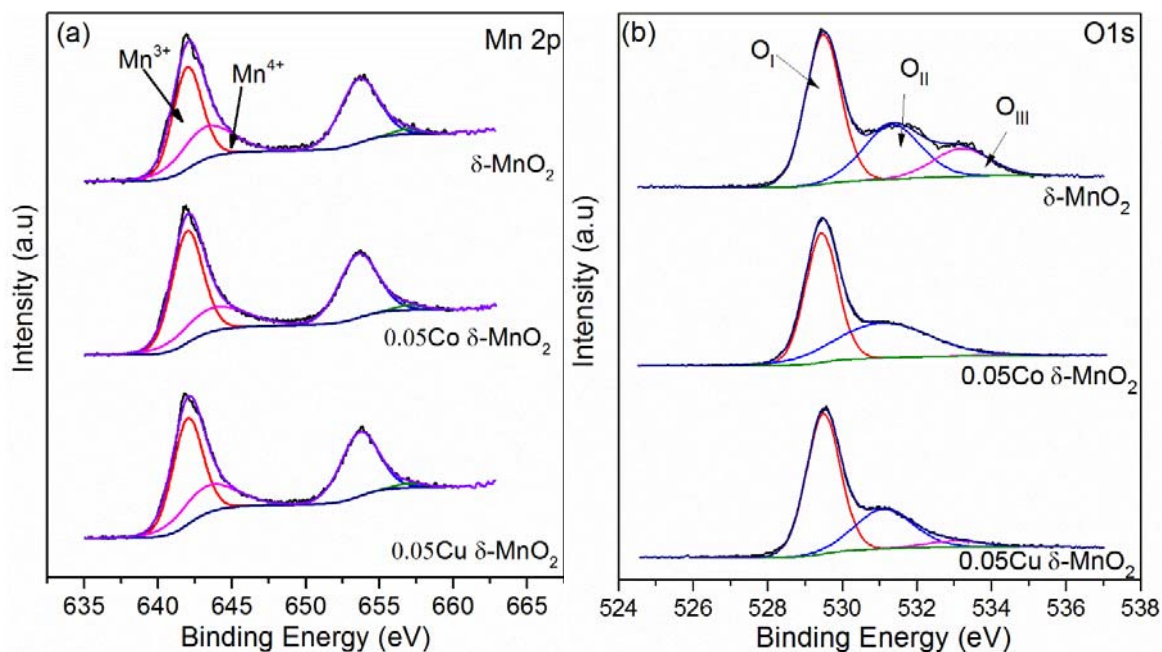


Figure 4. XPS Spectra of Mn 2P (a) and O 1s (b) of Pristine MnO₂, Co and Cu modified MnO₂

To further determine the effect of dopants on the nature and surface composition of oxygen species on the catalysts, the O1s spectrum was deconvoluted into three peaks, corresponding to lattice oxygen (O_I), surface active oxygen species (O_{II}) and surface adsorbed water molecules (O_{III}). The peaks located at 529.45 – 529.53 eV correspond to structural lattice oxygen (Mn-O-Mn), those at 531.09 – 531.34 eV are related to surface oxygen with low coordination which facilitates the formation of terminal hydroxyl groups (OH⁻) and defective-oxide surface adsorbed oxygen species (O⁻, O₂⁻), while the peaks at 533.1 – 533.4 eV can be attributed to surface adsorbed water molecules.^{11, 19} As seen in Figure 4(b), and Table 2, the relative amount of surface active oxygen species increases after the addition of dopants. Relative to the pristine δ -MnO₂, 0.05Co δ -MnO₂ exhibited an increase in the content of surface active oxygen species compared to 0.05Cu δ -MnO₂, in agreement with the deconvolution results of Mn 2p_{3/2} (Table 2) and HRTEM results. It is widely known that structural defects in the form of oxygen vacancies act as sites for the

activation of molecular oxygen and or water molecules into active or defective surface oxides and also enhance the mobility of lattice oxygen.^{8, 11, 42} This indicates that more Co^{3+} is incorporated into the lattice of $\delta\text{-MnO}_2$ compared to Cu^{2+} probably due to the coordination radius of the earlier being closer to that of Mn^{4+} compared to the latter,¹⁰ which leads to more structural distortion and the provision of sites for the generation of active oxygen species.

Moreover, a general increase in the intensity ratio of the Raman peaks (ν_1/ν_2) of the doped catalysts was observed. This might be indicative of the distortion in the Mn-O bond of the MnO_6 ,^{21, 39} and defects formation in the lattice framework of $\delta\text{-MnO}_2$ resulting from stress due to the incorporation of dopants into the lattice.^{22, 43} The intensity ratio of the (ν_1/ν_2) peaks is higher in 0.05Co $\delta\text{-MnO}_2$ than in 0.05Cu $\delta\text{-MnO}_2$, suggesting a higher level oxygen vacancies in the octahedral sheets in the presence of Co, further confirming the XPS, XRD and HRTEM results. A similar Raman technique was employed elsewhere to determine the extent of structural defect formation.⁴⁴⁻⁴⁵ Additionally, the FTIR results (Figure S3) showed more intense peaks around 3440, 1050 and 1633 cm^{-1} , which are respectively allocated to the stretching vibration of bound hydrates and OH^- groups in the interlayer structure of birnessite, and bending vibrations of O-H bonds of structural H_2O and OH groups,⁴⁶ further indicating the presence of more structural defects in 0.05Co $\delta\text{-MnO}_2$.¹⁹

Table 2. XPS analysis of Mn 2p_{3/2} and O1s

| Sample | Mn 2p _{3/2} | | $\text{Mn}^{4+}/\text{Mn}^{3+}$ | O1s center (eV) | | $\text{O}_{\text{II}}/\text{O}_{\text{total}}$ |
|-------------------------|----------------------|------------------|---------------------------------|-----------------|-----------------|------------------------------------------------|
| | Mn^{3+} | Mn^{4+} | | O _I | O _{II} | |
| MnO_2 | 642.0 | 643.3 | 0.65 | 529.5 | 531.3 | 0.31 |
| 0.05Co-MnO ₂ | 642.0 | 643.4 | 0.50 | 529.4 | 531.1 | 0.44 |
| 0.05Cu-MnO ₂ | 642.1 | 643.4 | 0.59 | 529.5 | 531.1 | 0.36 |

To understand the reduction behavior and further gain insight into the surface reducibility of the catalysts and the activity of the respective surface adsorbed oxygen and the effect of oxygen vacancies on oxygen mobility, the H₂ TPR profiles of the catalysts were collected and depicted in Figure 5. Only one broad peak with overlapping contributions corresponding to the reduction of surface active oxygen species and the successive reduction of MnO₂ was observed. The broad peak can be further divided into four peaks: α , β , γ and δ , respectively representing the reduction of surface adsorbed oxygen species (OH⁻, O⁻, O₂⁻) and the successive reduction of MnO₂ to Mn₂O₃, Mn₂O₃ to Mn₃O₄ and Mn₃O₄ to MnO.¹⁹

Although both the pristine MnO₂ and the doped catalysts exhibit similar reduction patterns, a slight shift of the reduction profile of the doped catalysts, to lower temperature, was observed compared to the pristine δ -MnO₂, as shown in Figure 5. Noticeably, the peak attributed to the reduction of surface active oxygen species shifted to around 150°C in the doped catalysts from 170°C in the pristine δ -MnO₂. Additionally, all the temperatures for the consecutive reduction of Mn from MnO₂ to MnO (β , γ and δ) decreased after doping, as depicted in Figure 5 and in Table 3. This suggests that the presence of dopants within the framework of δ -MnO₂ influences its reduction behaviour and mobility of lattice oxygen, likely due to electronic delocalization effect of the dopants¹⁷⁻¹⁸ and the formation of oxygen defects.^{19,37,42} This in agreement with the observed defect formation due to doping in the Raman, XPS and HRTEM results.

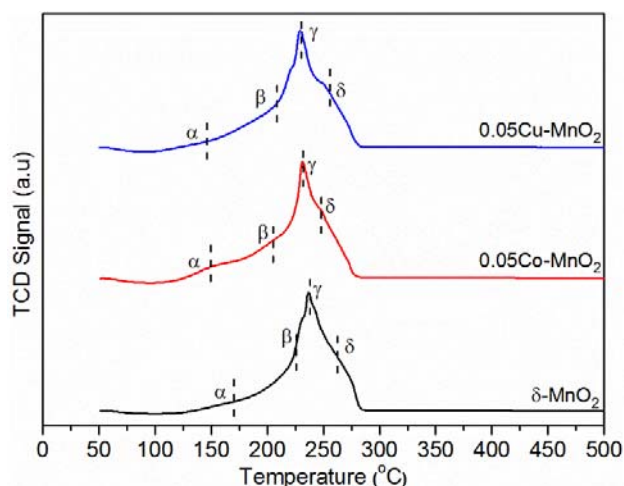


Figure 5. H₂-TPR of the investigated catalysts

Table 3. Catalytic activities (T_{50%} and T_{90%}) and H₂ reduction temperatures

| Sample | Temperature (°C) | | | | Catalytic activity | | Reaction rate (μmol.g ⁻¹ .min ⁻¹) | | Activation energy (kJ.mol ⁻¹) |
|---------------------------|------------------|-----|-----|-----|--------------------|------------------|----------------------------------------------------------|-------|-------------------------------------------|
| | α | β | λ | δ | T _{50%} | T _{90%} | 40°C | 70 °C | |
| δ-MnO ₂ | 170 | 225 | 237 | 265 | 74 | 87 | 0.091 | 0.266 | 40.9 |
| 0.05Co δ-MnO ₂ | 154 | 208 | 229 | 246 | 63 | 77 | 0.163 | 0.452 | 31.5 |
| 0.05Cu δ-MnO ₂ | 150 | 216 | 230 | 259 | 85 | 97 | 0.080 | 0.138 | 49.4 |

3.2 Catalytic Conversion of HCHO. The influence of dopants (Co and Cu) on the catalytic activity of the synthesized catalysts were evaluated under dynamic conditions (GHSV of 120,000 ml.g⁻¹.h⁻¹) for the complete conversion of HCHO (~170 ppm, ~50% RH). As seen in Figure 6a, the pristine δ-MnO₂ displayed a remarkably high activity and was able to achieve complete conversion of 170 ppm HCHO into CO₂ at 90°C. It is interesting to observe that after doping, 0.05Co δ-MnO₂ displayed enhanced catalytic activity while an opposite effect was observed on 0.05Cu δ-MnO₂, despite containing slightly more surface active species and displaying better reducibility than the pristine δ-MnO₂ catalyst. In the case of 0.05Co δ-MnO₂ higher catalytic

activity was observed over all temperature ranges and the temperature of complete conversion shifted down to 80°C from 90°C in the pristine δ -MnO₂, thereby indicating the promoting effect of Co on the catalytic activity of δ -MnO₂ for HCHO oxidation.

Conversely, 0.05Cu δ -MnO₂ showed reduced activity at almost all the temperature ranges, with complete conversion temperature moving up to 100°C. Interestingly, the difference between the catalytic activity of pristine δ -MnO₂ and that of 0.05Cu δ -MnO₂ increases with cumulative on-stream reaction time in spite of the increase in reaction temperature. Increasing the amount of doped Cu (0.1 and 0.2) led to further deterioration of catalytic activity, with no sign of catalytic over 0.2Cu δ -MnO₂ below 70°C (Figure S4), further demonstrating the observed inhibitory effect of Cu on the catalytic activity of δ -MnO₂. Although slight decrease in catalytic activity was observed with increasing Co doping ration from 0.05 to 0.2, all the Co doped catalysts exhibited improved catalytic activities relative to the pristine δ -MnO₂ (Figure S5). This could likely be due to the disruption of the layered structure of δ -MnO₂ at higher doping as seen in the XRD patterns (Figure S6). Similar observations were reported elsewhere for Co¹⁵ and Ce²² doped δ -MnO₂. For effective comparison, the temperatures for 50% (T_{50%}), 90% (T_{90%}) conversion and the reaction rates (40 and 70°C) are presented in Table 3. The T_{50%} for δ -MnO₂, 0.05Co δ -MnO₂ and 0.05Cu δ -MnO₂ are 74, 63 and 85°C respectively, while the T_{90%} are 87, 77 and 97°C respectively. As seen from Table 3, 0.05Co δ -MnO₂ showed the highest reaction rates over followed by the pristine δ -MnO₂. Besides, the values of the apparent activation energy (E_a) determined from the Arrhenius plots (Figure 6b) are 31.5, 40.9, and 49.4 kJ mol⁻¹ for 0.05Co δ -MnO₂, δ -MnO₂, and 0.05Cu δ -MnO₂ respectively, suggesting that HCHO is easily converted over 0.05Co δ -MnO₂.

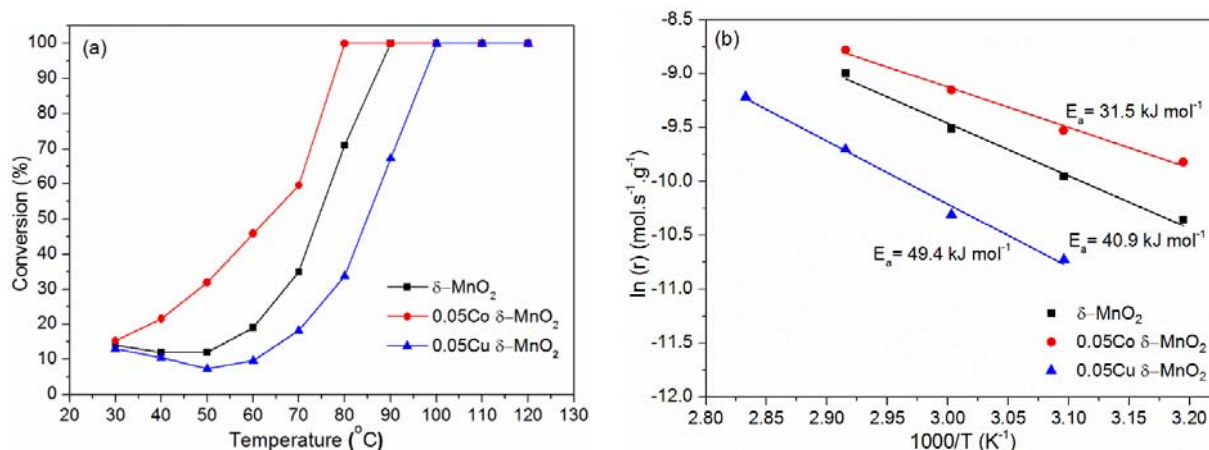


Figure 6. (a) Catalytic conversion of HCHO (170 ppm, ~50% RH, 120,000 ml·g⁻¹·h⁻¹) (b) Arrhenius plot for activation energy on the catalysts

To evaluate the activity of the catalyst under high throughput operation, the effect of GHSV on the activity of 0.05Co δ-MnO₂ was investigated under high space velocities of 120, 240 and 400 L·g⁻¹·h⁻¹, 170 ppm HCHO, and 45% RH. As depicted in Figure 7(a), the complete conversion temperature increases with increase in the GHSV from 80°C to 90 and 100°C for 120, 240 and 400 L·g⁻¹·h⁻¹ respectively. Even at high GHSV of 400 L·g⁻¹·h⁻¹, 0.05Co δ-MnO₂ was very active achieving complete conversion of HCHO at just 100°C. This further demonstrate the good catalytic activity of the catalyst. Next, to evaluate the suitability of the catalyst for application under typical indoor environment, the room temperature catalytic efficiency and stability of the catalyst were investigated under a feed concentration of ~10 ppm for 72 hrs in a dynamic system with a GHSV of 60 L·g⁻¹·h⁻¹ and presented in Figure 7(b). The results indicated an average conversion of up to 93.5% was sustained for 72 hrs on-stream. These results illustrate the stability of the catalyst, its high catalytic activity even under room temperature conditions and its suitability for the practical abatement of HCHO from indoor environment.

The increase in the surface concentration of the active oxygen species in the presence of dopants, particularly Co, suggests that the incorporation of dopants led to the generation of oxygen vacancies, which act as sites for the activation of molecular oxygen into active surface oxygen

species. It is clear from the characterization results that the remarkable activity of 0.05Co δ -MnO₂ is attributable to its abundant surface active oxygen species due to oxygen vacancies, and its relatively higher reducibility and mobility of lattice oxygen. Consumed surface active oxygen species could be regenerated by the interaction of structural defects with molecular oxygen and water molecules.¹⁸⁻¹⁹ The presence of oxygen vacancies could also enhance the mobility and activity of lattice oxygen to the surface, while molecular oxygen is activated into lattice oxygen at the oxygen vacant sites, thereby sustaining the whole process.^{22, 47}

Catalyst doping and or surface modification has been demonstrated to be an effective strategy for enhancing catalytic activity, mainly through the creation of defects and enriching the surface concentration of active oxygen species. Huang et al.⁹ observed improved activity over Eu doped CeO₂ with the highest surface concentration of defective oxides, which was attributed to the generation of oxygen vacancies due to the reduction of Ce. The generated vacant sites act as sites for the activation of oxygen into superoxides. The presence of surface defects improve the efficiency for hydroxylation reaction of benzene to phenol.⁴⁵ It was similarly demonstrated that the incorporation of W into MnO₂ led to the generation of oxygen vacancies and high surface concentration of reactive surface oxygen species, which in turn enhance the efficiency of the catalytic oxidation of HCHO.⁸ Correspondingly, Wang et al.¹¹ demonstrated that the presence of vacancies in the form of surface pores facilitated the formation of unsaturated oxygen and defective oxides, which significantly improve the catalytic activity of their investigated catalysts for HCHO oxidation. Liu et al.⁴¹ also established a direct relation between the oxygen vacancies density of ceria based catalysts to reactivity for CO oxidation.

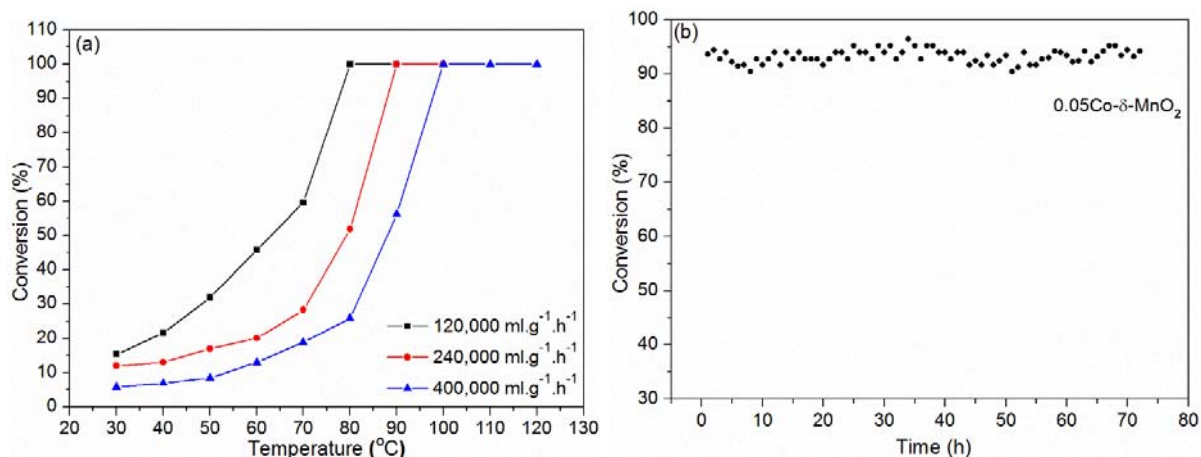


Figure 7. Effect of GHSV on catalytic activity of 0.05Co δ -MnO₂ (a), Room temperature and catalytic stability test of 0.05Co δ -MnO₂ 10 ppm, 60 L.g⁻¹.h⁻¹, 45% RH (b)

Note that the above results have clearly demonstrated that the ability of a dopant to create oxygen vacancies and facilitates the mobility of oxygen is a critical factor in enhancing the catalytic activity of δ -MnO₂ for HCHO oxidation. Such synergistic effect could be seen in the presence of Co. However, the inhibitory effect of Cu doping so far remains unclear, and the effect of surface area was ruled out, because the trend of surface area is not in agreement with that of the observed catalytic activities of the catalysts (Table S1). This observation is in agreement with previous works that showed that the oxidation of HCHO is not dependent on the surface area of the catalysts.^{5, 7, 22, 48} Next, DRIFTS analysis was conducted to understand if the type of dopant present has an impact on the surface reaction of δ -MnO₂, in terms of intermediate generation and desorption and/or accumulation. This will allow a better understanding of the promotional or inhibition effects of dopants.

4. REACTION MECHANISM

To further gain insights into the surface reaction mechanism of the HCHO oxidation and the influence of surface modification on the catalysts' reactivity, in situ DRIFTS analysis was conducted and the results are presented in Figure 8. In all the spectra, no peaks related to the C=O stretching band of surface adsorbed HCHO located at 1710cm⁻¹, was observed.⁴⁹ This suggests

that HCHO is immediately converted into intermediate species after adsorption. The strong absorption bands in the region of 3500 - 2900 cm^{-1} are assigned to strongly bonded hydroxyl groups.³⁵ Formates species as well as dioxymethylene species and carbonates were all observed as intermediates on all the investigated catalysts. The absorbance bands at 2830-2840 and 2865-2885 cm^{-1} (ν (CH) stretch), 1370-1373 cm^{-1} (δ (CH) bending), 1567-1580 cm^{-1} (ν_s (OCO)), and 1350-1352 cm^{-1} (ν_{as} (OCO)) are characteristics of formates species. The band splitting between the symmetric and asymmetric modes of C-O of formates is suggestive of the coordination of mode of formates on the surface. The splitting of 219, 225 and 227 cm^{-1} respectively for 0.05Co-, 0.05Cu-, and δ -MnO₂, is indicative of bridging mode coordination.^{35, 48, 50} The bands observed at 2730-2732, 1440-1453, and 1127-1161 cm^{-1} are characteristic features of dioxymethylene (DOM) species.^{6, 11, 48} Features attributed to bidentate carbonates (1653, 1240, and 1015-1053 cm^{-1}) and monodentate carbonates (1470-1490, 1315-1331 cm^{-1}) were also observed,^{7, 25, 51-53} while the bands at around 1620 cm^{-1} correspond to the bending vibration of adsorbed water molecules.⁵⁴⁻⁵⁵

In the presence of Co, the DOM species (1161 cm^{-1}) are quickly converted to formates intermediates, and exhibited the highest production rate of formates (1567 cm^{-1}). Furthermore, the carbonate feature at around 1498 and 1231 cm^{-1} are only present as weak shoulder on 0.05Co- δ -MnO₂, and the relative intensity of the carbonate peak at 1650 cm^{-1} is lower compared to other catalysts. This suggests that in the presence of Co, not only is HCHO quickly converted into its intermediate species but also are the intermediates quickly desorbed from the surface – freeing up active sites, leading to high catalytic activity, in agreement with its high reaction rates and lower activation energy (Table 3). This could likely be related to the enhanced lattice oxygen mobility and generation of surface active oxygen species induced by surface defects due to the incorporation of Co into the lattice structure of δ -MnO₂. Surface defective oxides and hydroxyl groups were

reported to take part in the formation of formates intermediates and further oxidation of surface carbonates into CO_2 .^{7, 51} On the other hand, it is interesting to observe that the carbonates peak (1653 cm^{-1}) on $0.05\text{Cu } \delta\text{-MnO}_2$ nearly became the dominant peak, thereby indicating the surface accumulation of carbonates with time. Furthermore, additional weak feature appeared at around 840 cm^{-1} on $0.05\text{Cu } \delta\text{-MnO}_2$, which is attributed to carbonate species.^{35, 53}

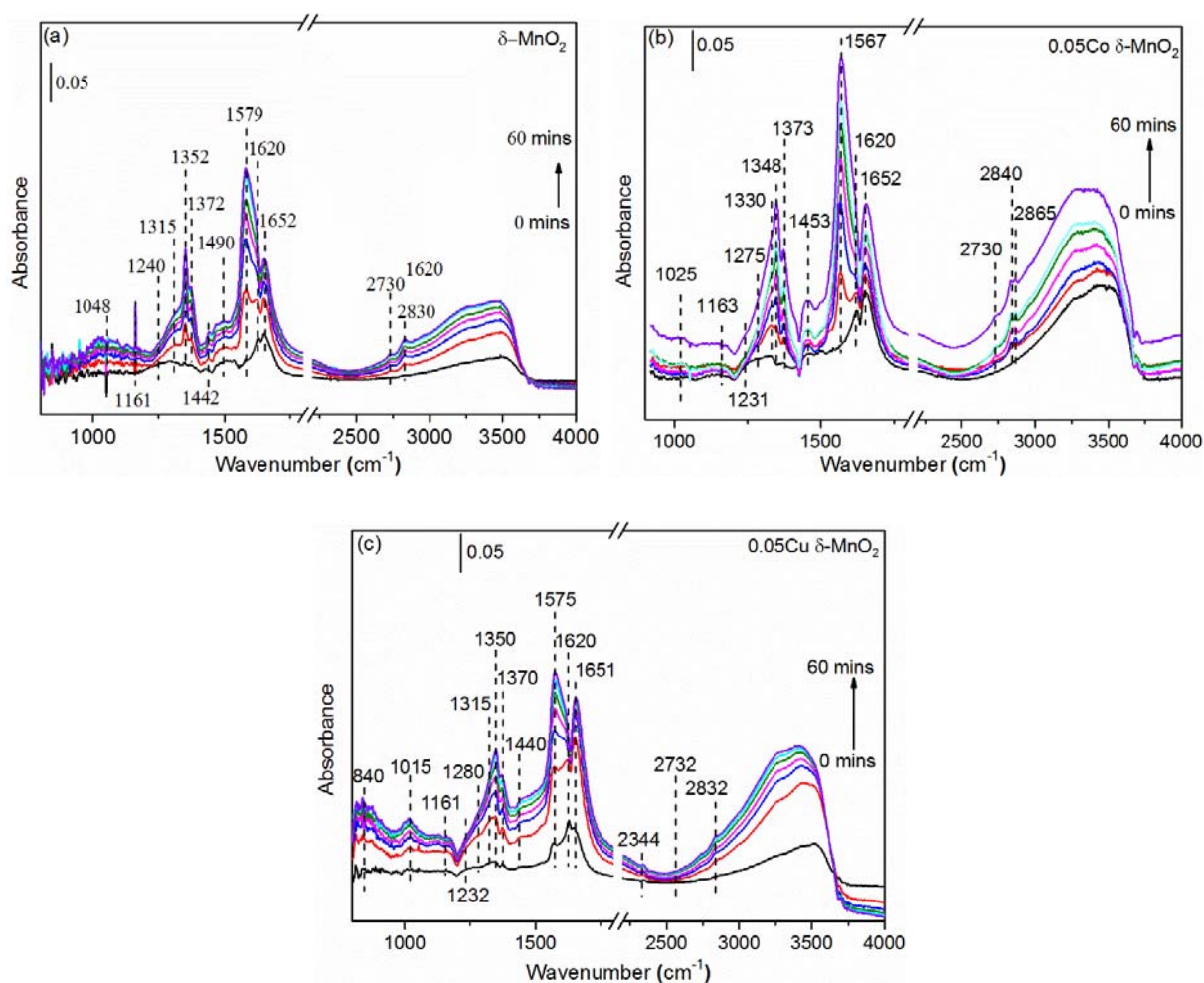


Figure 8. In situ DRIFTS results for (a) $\delta\text{-MnO}_2$ (b) $0.05\text{Co- } \delta\text{-MnO}_2$ (c) $0.05\text{Cu- } \delta\text{-MnO}_2$

To further ascertain this observation, the DRIFTS scans for $0.2\text{Cu } \delta\text{-MnO}_2$ at room temperature are presented in Figure S7. Compared to other catalysts, a remarkable weakening in the intensities of all the absorbance peaks were observed for the RT scans, indicating a poor RT performance, in

agreement with the activity test results (Figure S4). Moreover, the peaks attributed to carbonates species (1020 and 1646 cm^{-1}) dominated the entire spectra, which developed with time. The peaks related to formates appear very weak, notably, the asymmetric COO stretching peak of the formates (which is the dominant peak in other catalysts,) only appears as a weak shoulder band at 1580 cm^{-1} as depicted in Figure S7. This further supports the observed accumulation of carbonates on $0.05\text{Cu } \delta\text{-MnO}_2$ (Figure 8c) and could provide insights into the inhibitory effect of Cu on the activity of $\delta\text{-MnO}_2$, and the observed higher apparent activation compared to the pristine $\delta\text{-MnO}_2$. A plausible explanation could be related to the direct surface coordination between Cu and carbonates leading to surface accumulation and blockage of catalytic active sites. This could lead to steric hindrance for the reaction of HCHO with active sites, and a slowdown in catalytic activity, as observed in the catalytic conversion of HCHO over all Cu modified $\delta\text{-MnO}_2$ catalysts (Figure S4). It has been demonstrated that the presence of some dopants (La^{25} and Zr^{26}) could induce surface accumulation of carbonates, leading to the blockage of active sites and reduced catalytic activity for CO preferential oxidation,²⁵⁻²⁶ supposedly due to the thermal stability of the surface accumulated carbonates,²⁶ and hindrance of metal redox cycle and oxygen activation and mobility.²⁴ The high temperature DRIFTS results (Figure S8) illustrated that, as the reaction increases, the intensity of the surface accumulated carbonates attenuated (1646 cm^{-1}) while that of formates (asymmetric stretching of COO 1583 cm^{-1}) progressively increased until it became the dominant feature at 120°C (Figure S8 and S9). This suggests that as the carbonates desorb from the surface, more active sites are exposed and HCHO is converted into formates (evident by the increase in intensity at 1583 cm^{-1} in Figure S8). The hindrance effect of carbonates accumulation, in the presence of Cu, could be seen in the catalyst's inability to generate formate below 60°C (Figure S8). It is also noteworthy to mention that the oxidation of the carbonates into CO_2 and the

formation of formates, at elevated temperature, were accompanied by the consumption of surface hydroxyl groups (Figure S8). This indicates the participation of surface hydroxyl species in the oxidation of carbonates into CO₂.

In addition to surface hydroxyl groups, the main intermediates observed in the DRIFTS spectra of the investigated catalysts are DOM, formates and carbonates. The surface reaction of HCHO oxidation observed in the DRIFTS results (Figure 8) is illustrated in Figure 9, where M stands for dopant. The reaction first proceeds by the spontaneous adsorption of HCHO onto the surface of the catalyst and its conversion into DOM by surface active oxygen (evident by the absence of HCHO peaks). Formates intermediates could then be generated by the deprotonation of DOM, which further reacts to generate carbonate species.^{35, 56} A further reaction of the carbonates with surface hydroxyl group generates CO₂ and H₂O. The consumed hydroxyl groups are replenished by the reaction of water molecules with active oxygen species, while the surface active oxygen are replaced by the activation of molecular oxygen in the generated oxygen defects.^{7, 11-12} While the presence of Co enhances the oxidation of HCHO, the presence of Cu led to an inhibitory effect, as noted above.

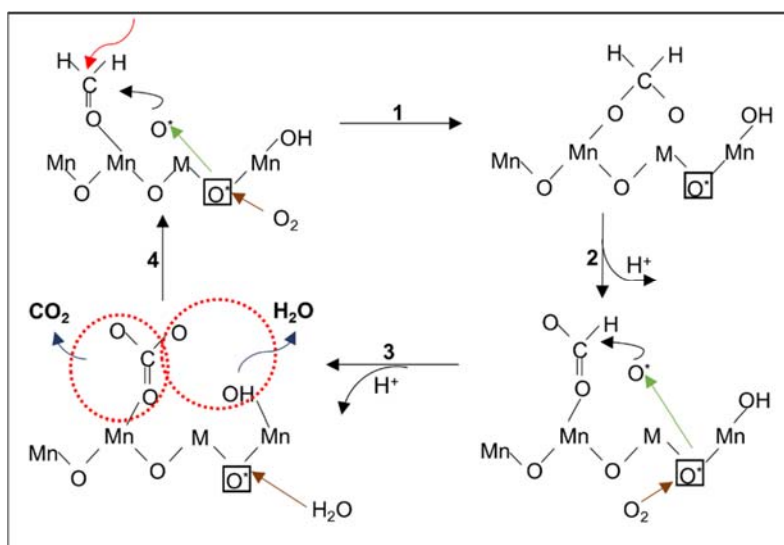


Figure 9. HCHO oxidation pathway on doped δ -MnO₂

On the basis of the above observations, it is therefore rational to state that the dopant-intermediate interaction is another critical parameter that affects catalytic activity. The presence of Cu in δ -MnO₂ leads to surface accumulation of carbonates, which in turn led to partial blockage of surface active sites, and likely hinder surface redox cycle and oxygen activation and mobility.²⁴
²⁶ This could explain why 0.05Cu δ -MnO₂ exhibited reduced catalytic, evidenced by lower reaction rates and HCHO conversion, and higher activation energy, despite possessing improved redox properties and relatively enriched surface active oxygen species, compared to the pristine δ -MnO₂. As such, for low-temperature oxidation of HCHO, desorption of carbonates from the catalysts' surface is a critical step to ensure availability of active sites for continuous reaction. Therefore, in addition to improving catalyst properties via doping for HCHO oxidation, the influence of the dopants on intermediates desorption from the catalyst's surface, particularly for low reaction temperature oxidation, in which case, not enough energy is applied to drive the desorption, is another critical parameter to be considered in designing catalysts for practical abatement of HCHO from indoor air environment.

5. CONCLUSION

Co and Cu dopants were explored for enhancing the catalytic activity of δ -MnO₂ for low-temperature HCHO oxidation. While defect generation was found to be of promotional effect, results suggests that dopants-intermediates interaction is another critical parameter that influences catalytic activity. The doping of Co into the lattice structure of δ -MnO₂ induced the generation of oxygen vacancies, enhanced its redox properties and oxygen mobility, and enriched the surface concentration of active oxygen species, leading to improved catalytic activity. Complete oxidation was achieved at 80°C. Additionally, room temperature oxidation of HCHO (~ 10 ppm), under dynamic conditions with an average conversion of about 93.5% over 72 hr was achieved. Although

improvement in redox properties and increment in surface concentration of active oxygen species was observed, the presence of Cu within the catalyst matrix led to suppression of catalytic activity. Surface accumulation of carbonates, in the presence of Cu, leading to the blockage of catalyst active sites, was identified as the main cause of activity suppression. These results demonstrate the influence of dopant on intermediates desorption and its importance in the design of catalysts for practical application, particularly for low-temperature reactions.

ASSOCIATED CONTENT

Supporting Information. The supporting information is available free of charge at <https://pubs.acs.org/> Co 2p XPS spectra, Cu 2p XPS spectra, FTIR spectra of catalysts, Effect of Co doping ratio on catalytic activity of δ -MnO₂, Effect of Cu doping ratio on catalytic activity of δ -MnO₂, XRD pattern of Co doped δ -MnO₂, Room temperature DRIFTS results for 0.2Cu δ -MnO₂, High temperature DRIFTS results for 0.2Cu δ -MnO₂, Effect of reaction temperature of the desorption of carbonates and formation of formates on 0.2Cu δ -MnO₂ (PDF)

AUTHOR INFORMATION

Corresponding Author

* Jun He - Department of Chemical and Environmental Engineering, University of Nottingham Ningbo China, Ningbo, China. Email: jun.he@nottingham.edu.cn

Author Contributions

The manuscript was written through contributions of all authors. All authors have given approval to the final version of the manuscript.

Notes

Authors declare no competing financial interest.

ACKNOWLEDGMENT

This work was carried out at the International Doctoral Innovation Centre (IDIC), University of Nottingham Ningbo, China. This work was supported by Ningbo Municipal Bureau of Science and Technology under the Innovation Team Project (2017C510001), Ningbo Municipal Bureau of Science and Technology Key Program (2019C10033 & 2019C10104), Start-up Research Funding of South-Central University for Nationalities (YZZ18018) and UK Engineering and Physical Sciences Research Council (EP/G037345/1 and EP/L016362/1).

6. REFERENCES

- (1) Shi, X.; Zhang, X.; Bi, F.; Zheng, Z.; Sheng, L.; Xu, J.; Wang, Z.; Yang, Y., Effective Toluene Adsorption over Defective UiO-66-NH₂: An Experimental and Computational Exploration. *J. Mol. Liq.* **2020**, *316*, 113812.
- (2) Bi, F.; Zhang, X.; Chen, J.; Yang, Y.; Wang, Y., Excellent Catalytic Activity and Water Resistance of UiO-66-Supported Highly Dispersed Pd Nanoparticles for Toluene Catalytic Oxidation. *Appl. Catal., B* **2020**, *269*, 118767.
- (3) Chen, J.; Zhang, X.; Shi, X.; Bi, F.; Yang, Y.; Wang, Y., Synergistic Effects of Octahedral TiO₂-Mil-101(Cr) with Two Heterojunctions for Enhancing Visible-Light Photocatalytic Degradation of Liquid Tetracycline and Gaseous Toluene. *J. Colloid Interface Sci.* **2020**, *579*, 37-49.
- (4) Zhang, X.; Song, L.; Bi, F.; Zhang, D.; Wang, Y.; Cui, L., Catalytic Oxidation of Toluene Using a Facile Synthesized Ag Nanoparticle Supported on UiO-66 Derivative. *J. Colloid Interface Sci.* **2020**, *571*, 38-47.
- (5) Yusuf, A.; Snape, C.; He, J.; Xu, H.; Liu, C.; Zhao, M.; Chen, G. Z.; Tang, B.; Wang, C.; Wang, J., Advances on Transition Metal Oxides Catalysts for Formaldehyde Oxidation: A Review. *Catal. Rev.: Sci. Eng.* **2017**, *59*, 189-233.
- (6) Yusuf, A.; Sun, Y.; Snape, C.; He, J.; Wang, C.; Ren, Y.; Jia, H., Low-Temperature Formaldehyde Oxidation over Manganese Oxide Catalysts: Potassium Mediated Lattice Oxygen Mobility. *Mol. Catal.* **2020**, *497*, 111204.
- (7) Wang, J.; Zhang, P.; Li, J.; Jiang, C.; Yunus, R.; Kim, J., Room-Temperature Oxidation of Formaldehyde by Layered Manganese Oxide: Effect of Water. *Environ. Sci. Technol.* **2015**, *49*, 12372-12379.

- (8) Liu, F.; Cao, R.; Rong, S.; Zhang, P., Tungsten Doped Manganese Dioxide for Efficient Removal of Gaseous Formaldehyde at Ambient Temperatures. *Mater. Des.* **2018**, *149*, 165-172.
- (9) Huang, Y.; Long, B.; Tang, M.; Rui, Z.; Balogun, M.-S.; Tong, Y.; Ji, H., Bifunctional Catalytic Material: An Ultrastable and High-Performance Surface Defect CeO₂ Nanosheets for Formaldehyde Thermal Oxidation and Photocatalytic Oxidation. *Appl. Catal., B* **2016**, *181*, 779-787.
- (10) Kwon, K. D.; Refson, K.; Sposito, G., Understanding the Trends in Transition Metal Sorption by Vacancy Sites in Birnessite. *Geochim. Cosmochim. Acta* **2013**, *101*, 222-232.
- (11) Wang, J.; Zhang, G.; Zhang, P., Layered Birnessite-Type MnO₂ with Surface Pits for Enhanced Catalytic Formaldehyde Oxidation Activity. *J. Mater. Chem. A* **2017**, *5*, 5719-5725.
- (12) Yang, W.; Zhu, Y.; You, F.; Yan, L.; Ma, Y.; Lu, C.; Gao, P.; Hao, Q.; Li, W., Insights into the Surface-Defect Dependence of Molecular Oxygen Activation over Birnessite-Type MnO₂. *Appl. Catal., B* **2018**, *233*, 184-193.
- (13) Elmacı, G.; Özgenç, G.; Kurz, P.; Zumreoglu-Karan, B., Enhanced Water Oxidation Performances of Birnessite and Magnetic Birnessite Nanocomposites by Transition Metal Ion Doping. *Sustainable Energy & Fuels* **2020**.
- (14) Ochirkhuyag, A.; Varga, T.; Tóth, I. Y.; Varga, Á. T.; Sági, A.; Kukovecz, Á.; Kónya, Z., Cost-Effective Ion-Tuning of Birnessite Structures for Efficient ORR Electrocatalysts. *Int. J. Hydrogen Energy* **2020**, *45*, 16266-16276.
- (15) McKendry, I. G.; Thenuwara, A. C.; Shumlas, S. L.; Peng, H.; Aulin, Y. V.; Chinnam, P. R.; Borguet, E.; Strongin, D. R.; Zdilla, M. J., Systematic Doping of Cobalt into Layered Manganese Oxide Sheets Substantially Enhances Water Oxidation Catalysis. *Inorg. Chem.* **2018**, *57*, 557-564.
- (16) Yin, H.; Feng, X.; Qiu, G.; Tan, W.; Liu, F., Characterization of Co-doped Birnessites and Application for Removal of Lead and Arsenite. *J. Hazard. Mater.* **2011**, *188*, 341-349.
- (17) Xia, G.; Yin, Y.; Willis, W.; Wang, J.; Suib, S., Efficient Stable Catalysts for Low Temperature Carbon Monoxide Oxidation. *J. Catal.* **1999**, *185*, 91-105.
- (18) Hernández, W. Y.; Centeno, M. A.; Ivanova, S.; Eloy, P.; Gaigneaux, E. M.; Odriozola, J. A., Cu-Modified Cryptomelane Oxide as Active Catalyst for Co Oxidation Reactions. *Appl. Catal., B* **2012**, *123-124*, 27-35.
- (19) Wang, X.; Huo, W.; Xu, Y.; Guo, Y.; Jia, Y., Modified Hierarchical Birnessite-Type Manganese Oxide Nanomaterials for Co Catalytic Oxidation. *New J. Chem.* **2018**, *42*, 13803-13812.
- (20) Dong, C.; Qu, Z.; Jiang, X.; Ren, Y., Tuning Oxygen Vacancy Concentration of MnO₂ through Metal Doping for Improved Toluene Oxidation. *J. Hazard. Mater.* **2020**, *391*, 122181.

- (21) Liu, Y.; Zong, W.; Zhou, H.; Wang, D.; Cao, R.; Zhan, J.; Liu, L.; Jang, B. W.-L., Tuning the Interlayer Cations of Birnessite-Type MnO₂ to Enhance Its Oxidation Ability for Gaseous Benzene with Water Resistance. *Catal. Sci. Technol.* **2018**, *8*, 5344-5358.
- (22) Zhu, L.; Wang, J.; Rong, S.; Wang, H.; Zhang, P., Cerium Modified Birnessite-Type MnO₂ for Gaseous Formaldehyde Oxidation at Low Temperature. *Appl. Catal., B* **2017**, *211*, 212-221.
- (23) Chen, L.; Jia, J.; Ran, R.; Song, X., Nickel Doping MnO₂ with Abundant Surface Pits as Highly Efficient Catalysts for Propane Deep Oxidation. *Chem. Eng. J.* **2019**, *369*, 1129-1137.
- (24) Gamarra, D.; Martínez-Arias, A., Preferential Oxidation of CO in Rich H₂ over CuO/CeO₂: Operando-Drifts Analysis of Deactivating Effect of CO₂ and H₂O. *J. Catal.* **2009**, *263*, 189-195.
- (25) Ke, J.; Xiao, J.-W.; Zhu, W.; Liu, H.; Si, R.; Zhang, Y.-W.; Yan, C.-H., Dopant-Induced Modification of Active Site Structure and Surface Bonding Mode for High-Performance Nanocatalysts: CO Oxidation on Capping-Free (110)-Oriented CeO₂: Ln (Ln= La–Lu) Nanowires. *J. Am. Chem. Soc.* **2013**, *135*, 15191-15200.
- (26) Davó-Quiñonero, A.; Navlani-García, M.; Lozano-Castelló, D.; Bueno-López, A.; Anderson, J. A., Role of Hydroxyl Groups in the Preferential Oxidation of CO over Copper Oxide–Cerium Oxide Catalysts. *ACS Catal.* **2016**, *6*, 1723-1731.
- (27) Zhou, L.; He, J.; Zhang, J.; He, Z.; Hu, Y.; Zhang, C.; He, H., Facile in-Situ Synthesis of Manganese Dioxide Nanosheets on Cellulose Fibers and Their Application in Oxidative Decomposition of Formaldehyde. *J. Phys. Chem. C* **2011**, *115*, 16873-16878.
- (28) Genuino, H. C.; Seraji, M. S.; Meng, Y.; Valencia, D.; Suib, S. L., Combined Experimental and Computational Study of CO Oxidation Promoted by Nb in Manganese Oxide Octahedral Molecular Sieves. *Appl. Catal., B* **2015**, *163*, 361-369.
- (29) Yin, H.; Kwon, K. D.; Lee, J.-Y.; Shen, Y.; Zhao, H.; Wang, X.; Liu, F.; Zhang, J.; Feng, X., Distinct Effects of Al³⁺ Doping on the Structure and Properties of Hexagonal Turbostratic Birnessite: A Comparison with Fe³⁺ Doping. *Geochim. Cosmochim. Acta* **2017**, *208*, 268-284.
- (30) Thenuwara, A. C., Cerkez, E.B., Shumlas, S.L., Attanayake, N.H., McKendry, I.G., Frazer, L., Borguet, E., Kang, Q., Remsing, R.C., Klein, M.L., et al., Nickel Confined in the Interlayer Region of Birnessite: An Active Electrocatalyst for Water Oxidation. *Angew. Chem., Int. Ed.* **2016**, *55*, 10381-10385.
- (31) Julien, C.; Massot, M.; Baddour-Hadjean, R.; Franger, S.; Bach, S.; Pereira-Ramos, J. P., Raman Spectra of Birnessite Manganese Dioxides. *Solid State Ionics* **2003**, *159*, 345-356.
- (32) Li, J.; Zhang, P.; Wang, J.; Wang, M., Birnessite-Type Manganese Oxide on Granular Activated Carbon for Formaldehyde Removal at Room Temperature. *J. Phys. Chem. C* **2016**, *120*, 24121-24129.

- (33) Sun, L.; Cao, Q.; Hu, B.; Li, J.; Hao, J.; Jing, G.; Tang, X., Synthesis, Characterization and Catalytic Activities of Vanadium–Cryptomelane Manganese Oxides in Low-Temperature NO Reduction with NH₃. *Appl. Catal., A* **2011**, *393*, 323-330.
- (34) Xiao, X.; Sun, S.-P.; McBride, M. B.; Lemley, A. T., Degradation of Ciprofloxacin by Cryptomelane-Type Manganese (III/IV) Oxides. *Environ. Sci. Pollut. Res.* **2013**, *20*, 10-21.
- (35) Li, C.; Domen, K.; Maruya, K.-I.; Onishi, T., Spectroscopic Identification of Adsorbed Species Derived from Adsorption and Decomposition of Formic Acid, Methanol, and Formaldehyde on Cerium Oxide. *J. Catal.* **1990**, *125*, 445-455.
- (36) Davis, D. J.; Lambert, T. N.; Vigil, J. A.; Rodriguez, M. A.; Brumbach, M. T.; Coker, E. N.; Limmer, S. J., Role of Cu-ion Doping in Cu-A-MnO₂ Nanowire Electrocatalysts for the Oxygen Reduction Reaction. *J. Phys. Chem. C* **2014**, *118*, 17342-17350.
- (37) Hou, J.; Li, Y.; Liu, L.; Ren, L.; Zhao, X., Effect of Giant Oxygen Vacancy Defects on the Catalytic Oxidation of OMS-2 Nanorods. *J. Mater. Chem. A* **2013**, *1*, 6736-6741.
- (38) Strauss, M.; Maroneze, C. M.; de Souza E Silva, J. M.; Sigoli, F. A.; Gushikem, Y.; Mazali, I. O., Annealing Temperature Effects on Sol–Gel Nanostructured Mesoporous TiO₂/SiO₂ and Its Photocatalytic Activity. *Mater. Chem. Phys.* **2011**, *126*, 188-194.
- (39) Thenuwara, A. C.; Shumlas, S. L.; Attanayake, N. H.; Cerkez, E. B.; McKendry, I. G.; Frazer, L.; Borguet, E.; Kang, Q.; Zdilla, M. J.; Sun, J., Copper-Intercalated Birnessite as a Water Oxidation Catalyst. *Langmuir* **2015**, *31*, 12807-12813.
- (40) Wang, W.-W.; Yu, W.-Z.; Du, P.-P.; Xu, H.; Jin, Z.; Si, R.; Ma, C.; Shi, S.; Jia, C.-J.; Yan, C.-H., Crystal Plane Effect of Ceria on Supported Copper Oxide Cluster Catalyst for CO Oxidation: Importance of Metal–Support Interaction. *ACS Catal.* **2017**, *7*, 1313-1329.
- (41) Liu, X.; Zhou, K.; Wang, L.; Wang, B.; Li, Y., Oxygen Vacancy Clusters Promoting Reducibility and Activity of Ceria Nanorods. *J. Am. Chem. Soc.* **2009**, *131*, 3140-3141.
- (42) Santos, V.; Soares, O.; Bakker, J.; Pereira, M.; Órfão, J.; Gascon, J.; Kapteijn, F.; Figueiredo, J., Structural and Chemical Disorder of Cryptomelane Promoted by Alkali Doping: Influence on Catalytic Properties. *J. Catal.* **2012**, *293*, 165-174.
- (43) Niu, X.; Lei, Z., Copper Doped Manganese Oxides to Produce Enhanced Catalytic Performance for CO Oxidation. *J. Environ. Chem. Eng.* **2019**, *7*, 103055.
- (44) Song, S.; Jiang, S.; Rao, R.; Yang, H.; Zhang, A., Bicomponent VO₂-Defects/MWCNT Catalyst for Hydroxylation of Benzene to Phenol: Promoter Effect of Defects on Catalytic Performance. *Appl. Catal., A* **2011**, *401*, 215-219.
- (45) Song, S.; Yang, H.; Rao, R.; Liu, H.; Zhang, A., Defects of Multi-Walled Carbon Nanotubes as Active Sites for Benzene Hydroxylation to Phenol in the Presence of H₂O₂. *Catal. Commun.* **2010**, *11*, 783-787.

- (46) Liang, S.; Teng, F.; Bulgan, G.; Zong, R.; Zhu, Y., Effect of Phase Structure of MnO₂ Nanorod Catalyst on the Activity for Co Oxidation. *J. Phys. Chem. C* **2008**, *112*, 5307-5315.
- (47) Tang, X.; Li, Y.; Huang, X.; Xu, Y.; Zhu, H.; Wang, J.; Shen, W., MnO_x-CeO₂ Mixed Oxide Catalysts for Complete Oxidation of Formaldehyde: Effect of Preparation Method and Calcination Temperature. *Appl. Catal., B* **2006**, *62*, 265-273.
- (48) Fan, Z.; Zhang, Z.; Fang, W.; Yao, X.; Zou, G.; Shangguan, W., Low-Temperature Catalytic Oxidation of Formaldehyde over Co₃O₄ Catalysts Prepared Using Various Precipitants. *Chinese J. Catal.* **2016**, *37*, 947-954.
- (49) Mao, C. F.; Vannice, M. A., Formaldehyde Oxidation over Ag Catalysts. *J. Catal.* **1995**, *154*, 230-244.
- (50) Durand, J. P.; Senanayake, S. D.; Suib, S. L.; Mullins, D. R., Reaction of Formic Acid over Amorphous Manganese Oxide Catalytic Systems: An in Situ Study. *J. Phys. Chem. C* **2010**, *114*, 20000-20006.
- (51) Fang, R.; Feng, Q.; Huang, H.; Ji, J.; He, M.; Zhan, Y.; Liu, B.; Leung, D. Y. C., Effect of K⁺ Ions on Efficient Room-Temperature Degradation of Formaldehyde over MnO₂ Catalysts. *Catal. Today* **2019**, *327*, 154-160.
- (52) Du, H.; Williams, C. T.; Ebner, A. D.; Ritter, J. A., In Situ Ftir Spectroscopic Analysis of Carbonate Transformations During Adsorption and Desorption of CO₂ in K-Promoted HTiC. *Chem. Mater.* **2010**, *22*, 3519-3526.
- (53) Evans, J.; Whateley, T., Infra-Red Study of Adsorption of Carbon Dioxide and Water on Magnesium Oxide. *Trans. Faraday Soc.* **1967**, *63*, 2769-2777.
- (54) Popova, G. Y.; Andrushkevich, T.; Chesalov, Y. A.; Stoyanov, E., In Situ Ftir Study of the Adsorption of Formaldehyde, Formic Acid, and Methyl Formiate at the Surface of TiO₂ (Anatase). *Kinet. Catal.* **2000**, *41*, 805-811.
- (55) Litke, A.; Su, Y.; Tranca, I.; Weber, T.; Hensen, E. J. M.; Hofmann, J. P., Role of Adsorbed Water on Charge Carrier Dynamics in Photoexcited TiO₂. *J. Phys. Chem. C* **2017**, *121*, 7514-7524.
- (56) Sekine, Y., Oxidative Decomposition of Formaldehyde by Metal Oxides at Room Temperature. *Atmos. Environ.* **2002**, *36*, 5543-5547.

TOC Graphic

